Available online at www.sciencedirect.com
ScienceDirect
Trans. Nonferrous Met. Soc. China 31(2021) 703−714
Transactions of Nonferrous Metals Society of China
www.tnmsc.cn

Corrosion behavior of copper in extremely harsh marine atmosphere in Nansha Islands, China

Xiao LU[1,2], Yu-wei LIU[1,2], Hong-tao ZHAO[2], Chen PAN[2], Zhen-yao WANG[2]

1. School of Materials Science and Engineering, University of Science and Technology of China, Shenyang 110016, China;
2. Institute of Metal Research, Chinese Academy of Sciences, Shenyang 110016, China

Received 10 April 2020; accepted 19 October 2020

Abstract: The corrosion behavior of pure copper exposed to the atmosphere of Nansha Islands for 21 months was studied by mass loss method, composition analysis, morphology observation and electrochemical measurements. The results showed that the average corrosion rate of copper exposed for one year was approximately 7.85 μm/a, implying that Nansha Islands was classified as a corrosion category of CX. The structure and properties of the corrosion product layer generated on the front and back sides of the exposed sample differed significantly. The inner corrosion product layer (Cu_2O) on the front side was relatively thick and dense, whereas the outer product layer ($Cu_2Cl(OH)_3$) was extremely thin. However, the outer product layer on the back side was thicker than the inner layer. Electrochemical measurements indicated that the protection afforded by the corrosion product layer on the front side was improved gradually, while that on the back side was deteriorated.

Key words: copper; field exposure; mass loss; atmospheric corrosion; Nansha Islands

1 Introduction

As important functional materials, copper and its alloys are widely used in communications, electronic components and outdoor buildings. Similar to other metal materials, their atmospheric corrosion is a complex physical and chemical process, and essentially, an electrochemical reaction under a thin liquid film [1], which is mainly affected by environmental parameters such as temperature, relative humidity, and pollutants in the atmosphere.

In recent years, many studies have been carried out to investigate atmospheric corrosion of copper through various typical outdoor exposures [2−4]. The corrosion data can reflect the real corrosion behavior of copper in atmospheric environments. Cu_2O is typically the corrosion product first formed independently of the exposure conditions; hence, it is always present on the surface of pure copper [5−8]. Cu_2O can react with pollutants in the atmosphere to form different basic copper salts. In general, in urban, industrial and rural atmospheres, basic sulfates are the predominant components [9−12], while basic chlorides dominate in marine atmospheres [13−15]. The characteristics of the corrosion products formed on the metal surface affect their long-term corrosion rate. Numerous outdoor exposure experiments have shown that the atmospheric corrosion rate of copper is the highest in the initial years of exposure, and then decreases and stabilizes over time. This is mainly due to the formation of protective corrosion products on the surface of copper. However, it was found that the morphology and crystallization

Corresponding author: Zhen-yao WANG; Tel/Fax: +86-24-23893544; E-mail: zhywang@imr.ac.cn
DOI: 10.1016/S1003-6326(21)65531-0

degree of the corrosion products are also factors that increase the corrosion rate of copper under sheltered coastal conditions with time [13]. In addition to the properties of the metal, the factors affecting the atmospheric corrosion of copper include temperature, relative humidity, rainfall and corrosion media (such as SO_2, NO_2, O_3 and Cl^-). Atmospheric corrosion usually occurs under the synergistic effect of these factors. KONG et al [16,17] found that deposits on copper in hot and dry atmosphere in Turpan improved its resistance to corrosion, but the protection performance decreased with the increase of temperature. AN et al [18] found that rainfall significantly accelerated the corrosion rate of copper exposed to the atmosphere in Shenyang, China. SU et al [10] conducted the exposure tests for copper in Zhanjiang and Zhuhai, and their results showed that the corrosion behavior of copper exposed to different atmospheric environments was different. These results illustrate that atmospheric environment plays an important role in the corrosion behavior of copper.

Nansha Islands are located in the southern part of the South China Sea, belonging to marine tropical rainforest climate. Affected by the ocean, the temperature varies little throughout the year, with an annual average of 28.1 °C. The relative humidity is high, with an average of 79%, and the amount of rainfall is abundant, reaching 2000 mm per year. The average deposition rate of chloride is 1154.25 mg/(m^2·d), which is the S_3 level in ISO 9223. Therefore, Nansha has a typical harsh marine atmospheric environment characterized by high temperature, high humidity and high salt. Owing to severe weather conditions, the metal materials used in the construction of islands and reefs in the South China Sea face a serious risk of atmospheric corrosion. To date, the corrosion data for pure copper subjected to the specific atmospheric environment of Nansha have not been reported. To obtain accurate and current information about copper corrosion in Nansha, it is essential to conduct field exposure experiments for copper in Nansha Islands.

In this work, the corrosion process of pure copper exposed to the environmental conditions of Nansha was examined using the mass loss method, X-ray diffractometry, scanning electron microscopy and electrochemical measurements. The results of this study will provide more real and effective corrosion data for the application of copper in Nansha Islands.

2 Experimental

2.1 Sample preparation

The material exposed on the site was copper T2 (≥99.70 wt.% Cu). All sample coupons were 200 mm × 100 mm × 3 mm in size. Prior to the exposure to the atmosphere, they were degreased ultrasonically in acetone, rinsed with deionized water, dehydrated with alcohol, dried by cold air and stored in a desiccator.

2.2 Field exposure

The samples were exposed to environmental conditions of Nansha Islands, by placing them at an angle of 45° on a sample shelf, with the front side facing up and the back side facing down, in accordance with GB 11112 — 89. The exposure began in September 2017, with sampling periods of 2, 5, 13 and 21 months, respectively.

2.3 Mass loss

Mass loss is a proven measure of corrosion damage. It can be obtained by subtracting the mass of the sample after removing the corrosion products from the original mass before exposure. To determine the corrosion rate of the samples for different exposure periods, the average values of three parallel samples were taken for each exposure period. The removal of corrosion products from the surface of the sample was conducted in accordance with ISO 8407. First, the sample surface was cleaned with deionized water, following which the remaining corrosion product was removed by immersion in a specific solution (100 mL H_2SO_4 + 900 mL deionized water) for 1−3 min at 20−25 °C. Finally, the sample was rinsed with deionized water, dehydrated with alcohol and dried by cold air before being weighed by an electronic balance to determine the mass loss. In addition, the mass loss during rust removal was corrected with the unexposed specimens.

2.4 Characterization

After the samples were retrieved, the corrosion products formed on the surface of the samples were analyzed and characterized by various methods.

The macroscopic morphologies of the corroded specimens were observed using a digital camera. The cross-sectional micro-morphologies of the samples were examined by SEM at 20 kV and energy dispersive spectroscopy (EDS). The chemical composition and phase structure of the corrosion products were identified by X-ray photoelectron spectroscopy (XPS) and XRD. The phases present were identified using the Joint Committee on Powder Diffraction Standards (JCPDS) database.

2.5 Electrochemical measurements

Potentiodynamic polarization and electrochemical impedance spectra (EIS) were performed using an electrochemical workstation (PARSTAT 2273) to analyze the protective nature of the corrosion product layer formed on the sample. In the present work, the exposed samples, flat platinum plate and saturated calomel electrode (SCE) were served as the working electrode, counter electrode and reference electrode, respectively. In order to reduce the error caused by the uneven surface of the entire sample and ensure the reliability of the obtained data, at least three different positions were measured for each sample with different exposure periods. Subsequently, the electrochemical results of the sample were selected from the experimental data with good reproducibility. The surface area of the working electrode was 1 cm^2. All tests were conducted in a three-electrode electrolytic cell with a 3.5% NaCl solution. Before the polarization and EIS experiments, the open circuit potential (OCP) was measured for 15 min to stabilize the system. The scanning rate of the potentiodynamic polarization measurements was 20 mV/min. EIS measurements were carried out at OCP in the frequency range from 1×10^5 to 1×10^{-2} Hz, and the potential disturbance amplitude was 10 mV.

3 Results

3.1 Corrosion kinetics

The deterioration of the materials was evaluated in every sampling cycle by measuring the mass loss in triplicate. In order to obtain a clearer view of the corrosion damage, the mass loss of the exposed samples was converted to the loss of thickness. Figure 1 shows the variations in the average thickness loss as a function of exposure time. The corresponding fitting formula for the measured data is as follows:

$$D=a+bt=1.3917+6.4632t \quad (1)$$

where D (in μm) represents the loss of thickness after exposure time t (in a), a and b are constants. The thickness loss of the copper samples was found to obey a linear increase during the 21 months of exposure.

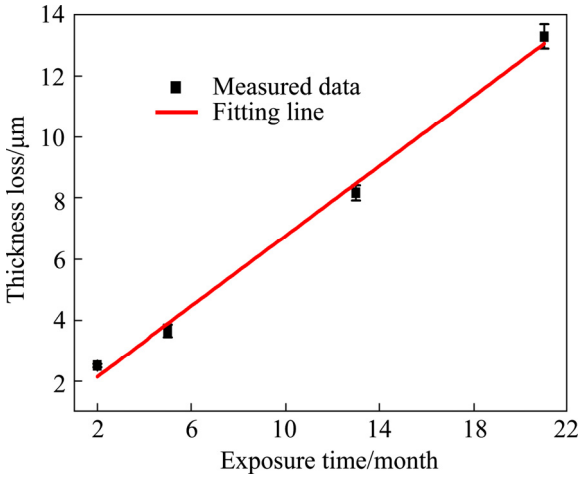

Fig. 1 Thickness loss of copper exposed to Nansha marine atmosphere as function of exposure time

It can be determined from Eq. (1) that the average corrosion rate of copper exposed for one year was approximately 7.85 μm/a. According to ISO 9223, Nansha was classified in corrosion category of CX (5.6−10 μm/a). In addition, the one-year average corrosion rates of copper T2 exposed to other marine climate exposure sites is shown in Fig. 2 [19]. The climate of Wanning is characterized by strong winds and a short dew time. Moreover, the average Cl^- deposition rate of Qingdao and Wanning is far lower than that of Nansha. Therefore, compared with other exposure fields, the relatively high temperature, relative humidity, rainfall and Cl^- deposition in Nansha accelerated the copper corrosion, confirming that the atmospheric environment of Nansha is an extremely harsh corrosive environment.

3.2 Macroscopic morphology

The surface color of the exposed samples changed after exposure to the Nansha marine atmosphere. The macroscopic morphologies of the copper samples exposed for different periods are

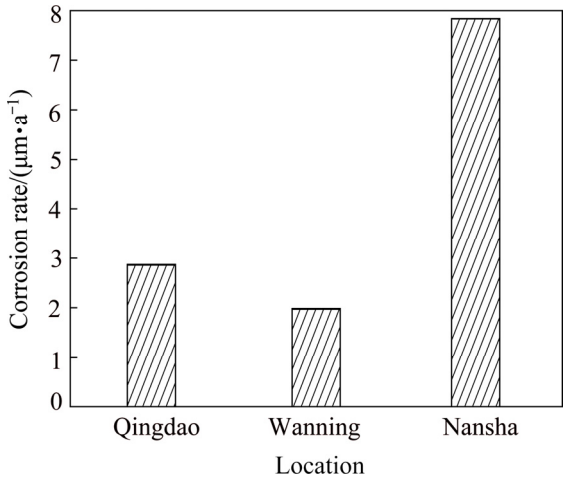

Fig. 2 Average corrosion rates of copper T2 during one year of exposure at several marine climate exposure sites [19]

displayed in Fig. 3. Significant differences in the morphologies of the front and back sides of the exposed samples were observed.

Macroscopically, the corrosion product layer on both sides of the copper sample had a double-layered structure. On the front side, uneven bluish green corrosion products were generated on the brownish red corrosion products of the inner layer after two months of exposure. As the exposure time increased, the inner layer gradually turned brown, and the amount of bluish green corrosion products gradually increased, but was significantly less than the amount of bluish green corrosion products on the back side. On the back side, the inner layer also gradually changed from brownish red to brown, but the bluish green corrosion products grew faster and connected to become the loose outer layers. Furthermore, after 13 months of exposure, a small amount of black compounds appeared in the bluish green corrosion products. After 21 months, large masses of black compounds were observed on the back side. These results indicate that the corrosion mechanism of the front and back sides of the exposed sample might be different.

3.3 Composition of corrosion products

The phase compositions of the corrosion products formed on the surface of copper exposed to the Nansha marine atmosphere for different periods are presented in Fig. 4. The XRD results indicate that the corrosion products on copper were mainly Cu_2O (PDF 99-0041) and $Cu_2Cl(OH)_3$ (PDF 87-0679), which corresponded to the brown and bluish green corrosion products observed in the macroscopic morphologies, respectively. It can also be found that the peaks of CuO (PDF 89-5899) began to appear after 13 months of exposure. After 21 months of exposure, the number of CuO peaks detected on the back side increased, and the intensities of the CuO and Cu_2O peaks were significantly higher than those on the front side, which explains why part of the area on the back side of the exposed sample was observed to blacken after 13 months of exposure. Cu_2O is the main corrosion product of copper exposed to the atmosphere, while $Cu_2Cl(OH)_3$ is generated by the interaction between Cu_2O and Cl^- under the water film when the concentration of Cl^- is high in the atmosphere, particularly in the marine environment.

To confirm the compositions of the corrosion products more accurately, high-resolution Cu 2p spectra for the front and back sides of the samples exposed for 21 months were obtained, as shown

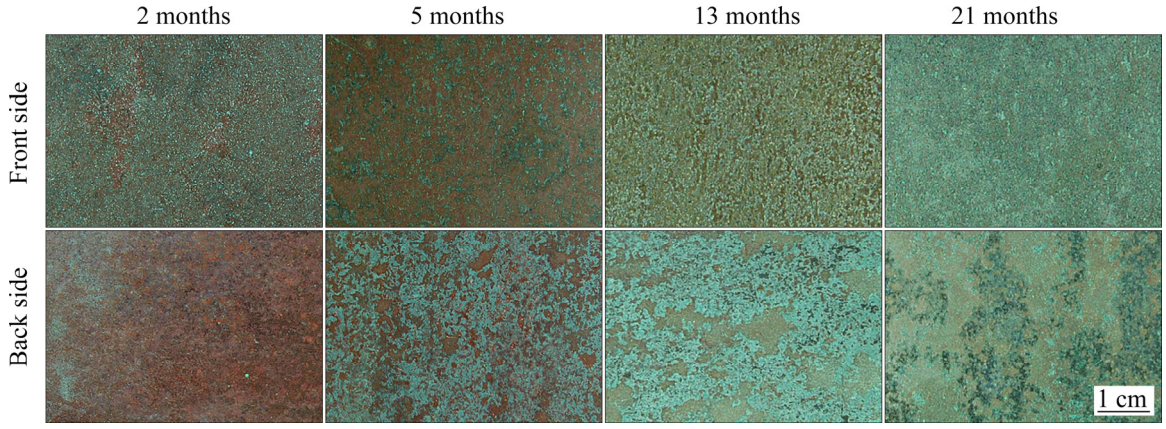

Fig. 3 Macroscopic morphologies of copper exposed in Nansha marine atmosphere for different periods

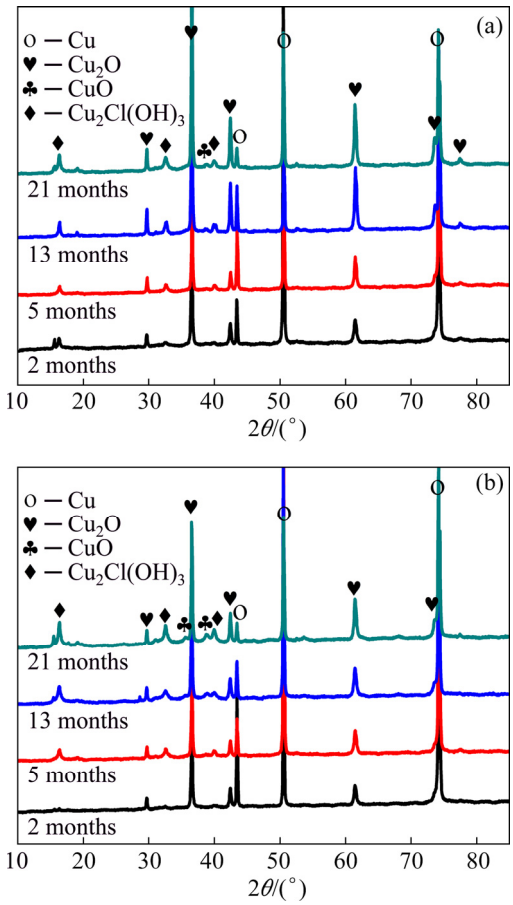

Fig. 4 XRD patterns of copper exposed in Nansha marine atmosphere for different times: (a) Front side; (b) Back side

in Fig. 5. Remarkably, the Cu 2p spectra showed the $2p_{3/2}$ peak at 932.9 eV and the $2p_{l/2}$ peak at 952.8 eV. The core-level Cu $2p_{3/2}$ spectra were recorded in binding energy range of 926–937 eV for the front and back sides and are presented in Figs. 5(b, c), respectively. Peaks at binding energies of 932.50, 933.60 and 934.56 eV correspond to Cu_2O, CuO and Cu(II), respectively [16,20,21]. This result is consistent with the XRD results and confirms the presence of CuO. The fitting parameters for the XPS spectra in Fig. 5 and the relative quantity of compounds in the corrosion layers of the exposed samples are listed in Table 1. The major constituent of the corrosion product layer on the front side is Cu_2O. However, the amount of the three phase components of the corrosion product layer on the back side is relatively average, which indicates that the component of the corrosion product layer on the back side of the sample after 21 months of exposure is mainly composed of Cu_2O, CuO and $Cu_2Cl(OH)_3$.

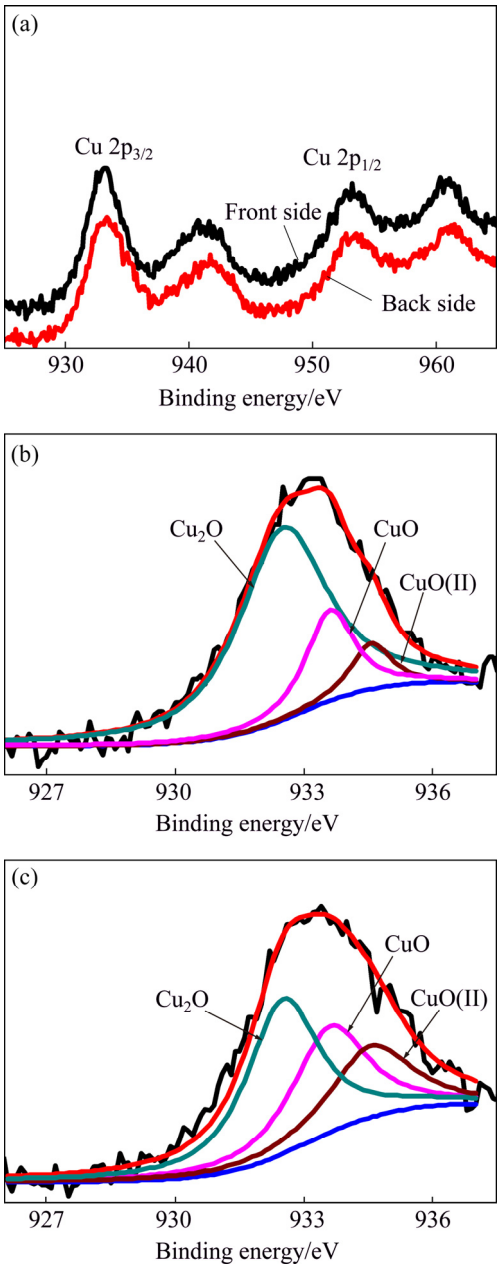

Fig. 5 XPS spectra of corrosion product layer on surface of copper exposed for 21 months: (a) Cu 2p spectra of corrosion product layer; (b) Core-level Cu $2p_{3/2}$ spectrum for front side; (c) Core-level Cu $2p_{3/2}$ spectrum for back side

3.4 Micromorphology

The corrosion product layer generated on the surface of the sample has a direct impact on the corrosion sensitivity of the metal, which may act as a diffusion barrier to prevent the migration of the corrosive electrolyte to the metal surface, or produce a diffusion channel to accelerate the immersion of the corrosive medium. Therefore, it is necessary to study the structure of the formed

corrosion product layer and relate it to the corrosion properties of the metal.

Figure 6 shows the evolution of the cross-sectional morphology of the copper samples exposed in Nansha marine atmosphere for different periods. It can be clearly seen that the corrosion product layers formed on both sides of copper gradually thickened with prolonged exposure, in the form of a double-layered structure. The difference is that the outer corrosion product layer on the front side was extremely thin and the inner layer was very thick, while the outer layer of the corrosion product on the back side was thicker than the inner layer. In addition, the corrosion product layer on the front side was very compact and dense and had a good combination with the substrate, while obvious transverse cracks appeared on the back side, resulting in poor adhesion between the corrosion product layer and the substrate.

The distribution of elements on the front and back sides of copper exposed for 21 months was scanned to analyze the composition of the double-layer, as shown in Fig. 7. The Cl element was mainly concentrated in the outer corrosion product layer, indicating that the outer layer was chlorine-containing compound of copper. Combined with the XRD and XPS results, it can be concluded that the outer corrosion products on the surface of copper were mainly $Cu_2Cl(OH)_3$ and the inner corrosion products were copper oxide (Cu_2O).

Table 1 Fitting parameters for Cu $2p_{3/2}$ XPS spectra in Fig. 5

Exposed sample	Chemical state	Binding energy/eV	FWHM/eV	Area	Relative quantity
Front side	Cu_2O	932.50	2.34	28082.79	0.732
	CuO	933.60	1.33	7247.285	0.189
	Cu(II)	934.56	1.1	3036.416	0.079
Back side	Cu_2O	932.50	2	15876.78	0.451
	CuO	933.60	2.06	11191.57	0.318
	Cu(II)	934.56	2.22	8099.095	0.231

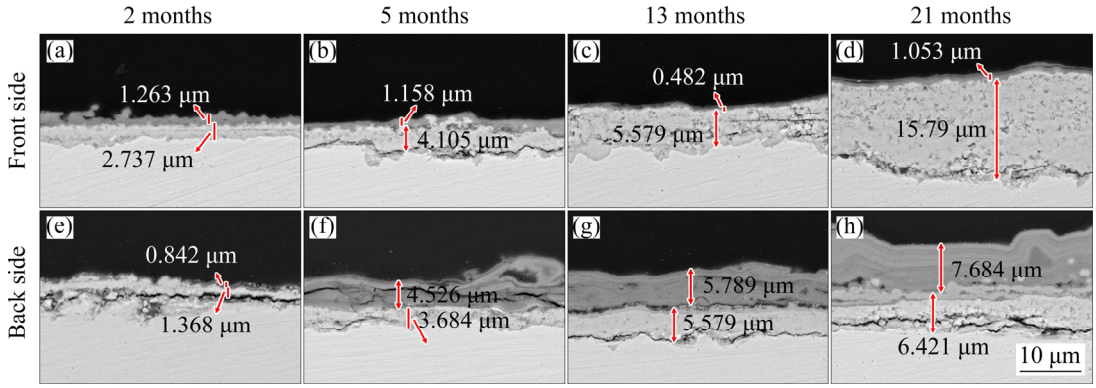

Fig. 6 Cross-sectional morphologies of copper exposed in Nansha marine atmosphere for different periods

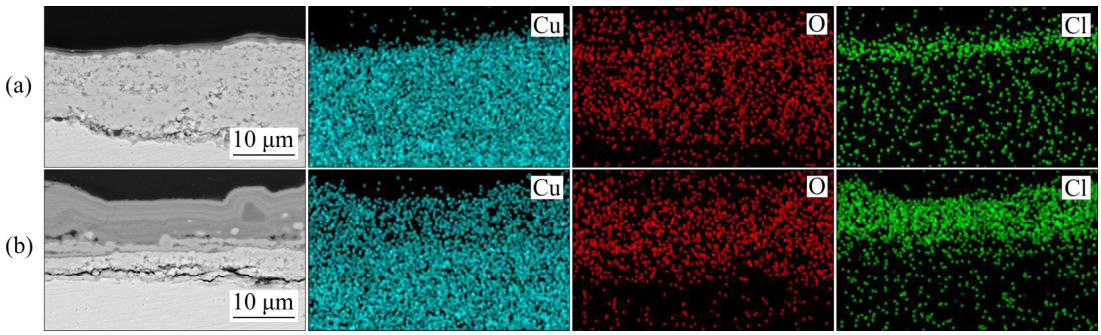

Fig. 7 Element distributions on cross-section of copper exposed for 21 months: (a) Front side; (b) Back side

This indicates that the corrosion products that covered the front side were primarily composed of Cu_2O.

3.5 Electrochemical results

Potentiodynamic polarization was performed on the front and back sides of copper to assess the anti-corrosion performance of the corrosion product layers. Figure 8 displays the polarization curves for different exposure times. The polarization curves of the exposed samples presented similar shapes, which implies that the polarization behavior of copper did not change at different exposure time. When the cathodic overpotential is not very high, oxygen reduction is the main reaction on the electrode [22−24]; thus, for the copper samples exposed to the Nansha atmosphere, the anodic process is the metal dissolution reaction and the cathodic process is the reduction of O_2.

The corresponding electrochemical parameters deduced by Tafel fitting are listed in Table 2. The corrosion current density (J_{corr}) can be used to estimate the kinetics of the overall corrosion process [25−28]. The results show that the corroded

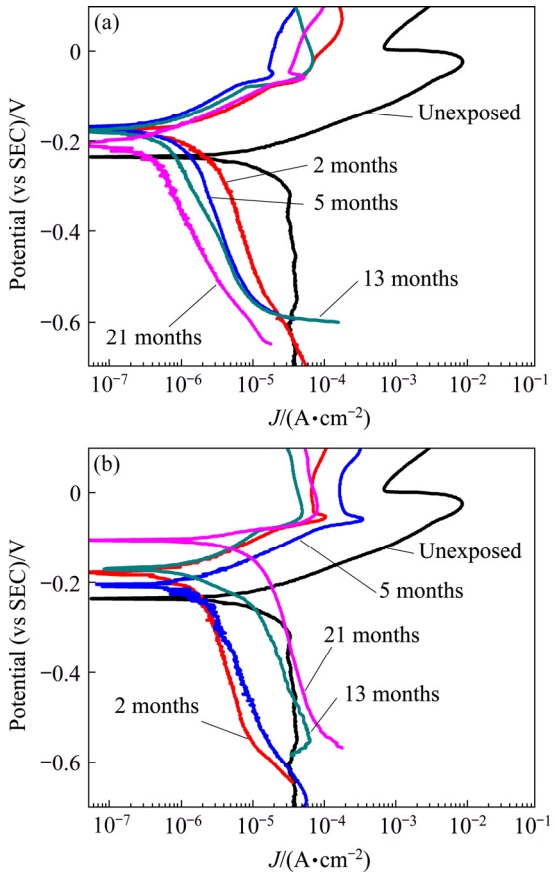

Fig. 8 Polarization curves of copper exposed for different time: (a) Front side; (b) Back side

Table 2 Tafel fitting results of polarization curves shown in Fig. 8

Exposed sample	Exposure time/months	φ_{corr}(vs SCE)/mV	J_{corr}/(μA·cm^{-2})
–	0	−235.04	11.54
Front side	2	−180.01	1.344
	5	−170.64	0.813
	13	−177.97	0.664
	21	−206.37	0.384
Back side	2	−178.29	1.239
	5	−207.04	1.375
	13	−169.41	2.111
	21	−105.41	4.663

samples exposed for different periods exhibited lower corrosion current densities than the unexposed sample, indicating that the corrosion product layers formed on the surface of copper could provide certain protection in the Nansha marine environment. In addition, it is of particular interest to note that the variation trend of the corrosion current density on the front and back sides of the samples was significantly different. The J_{corr} value on the front side of copper decreased gradually with prolonged exposure, which indicates that the corrosion rate on the front side of the sample decreased gradually, that is, the protective effect of the corrosion product layer on the substrate was gradually enhanced. In contrast, the back side showed a reverse trend, suggesting that the corrosion rate on the back side of the sample increased gradually and the protection of the corrosion product layer was gradually weakened. Thus, it can be understood that the overall corrosion rate of copper, as measured by the mass loss method, remained essentially unchanged. These results show the complexity of the overall corrosion process of copper exposed to the Nansha marine atmosphere and demonstrate that the corrosion products on the front and back sides had a profound impact on both the corrosion rate and corrosion mechanism.

In order to interpret the structure and corrosion resistance of the corrosion products formed on the sample surface, EIS measurements were conducted on both sides of copper exposed to Nansha for different periods. The Nyquist and Bode plots are shown in Fig. 9. The impedance measured on the

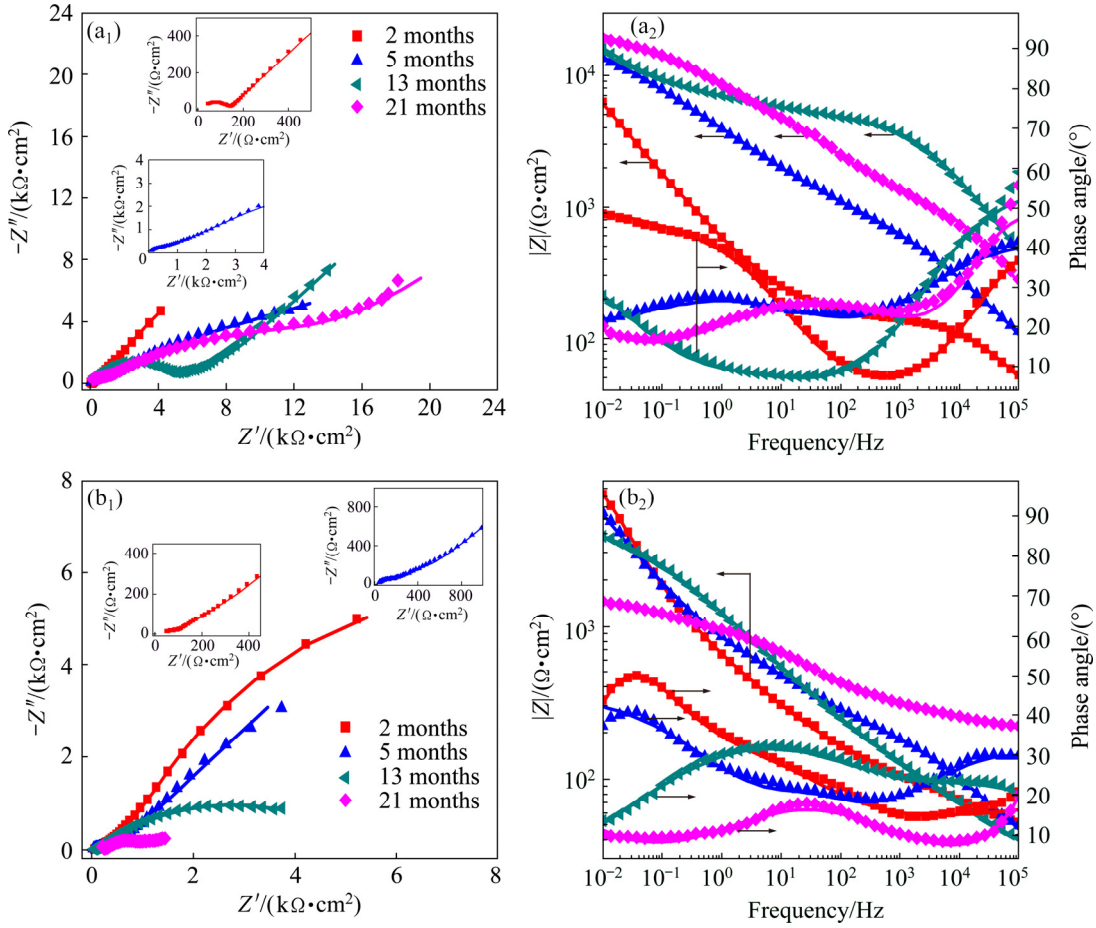

Fig. 9 Nyquist (a_1, b_1) and Bode (a_2, b_2) plots of copper exposed for different time: (a_1, a_2) Front side; (b_1, b_2) Back side

front side showed a tail corresponding to the Warburg impedance in the low-frequency region during the whole corrosion process (Fig. 9(a_1)), which indicates the occurrence of diffusion process on the sample surface, including the anodic diffusion of soluble metal species from the surface to solution and the cathodic diffusion of dissolved oxygen in the opposite direction [24,29,30]. However, the Warburg impedance was measured only after 21 months of exposure for the back sides (Fig. 9(b_1)), indicating that the diffusion process played an important role in the electrode reaction at the later stage of exposure.

Considering the features of the Nyquist plots and cross-sectional morphologies, the equivalent circuit models used to fit the experimental impedance data are presented in Fig. 10. The two capacitive arcs in series (Fig. 10(a)) were used to interpret the sub-electrochemical structure of the corrosion products formed on the front sides. Parallel capacitive arcs (Figs. 10(b, c)) were used to fit the data of the back sides. In the models, R_s is the

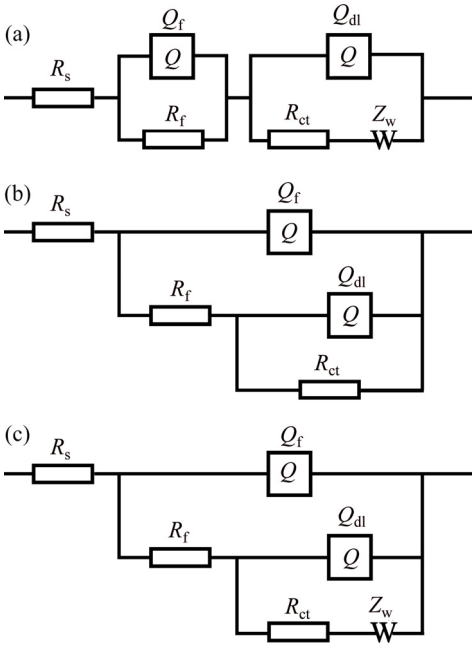

Fig. 10 Equivalent circuit models used to fit experimental impedance data of exposed samples: (a) Front side; (b) Back side without displaying Warburg impedance; (c) Back sides displaying Warburg impedance

solution resistance; Q_f and R_f represent the capacitance and resistance of the corrosion product layer, respectively; Q_{dl} and R_{ct} correspond to the double-layer capacitance and charge transfer resistance, respectively; Z_w is the Warburg impedance appearing in the low-frequency region. When fitting data by the circuits, the Chi-squared values were on the order of 10^{-3}, and the corresponding fitted data shown in Fig. 9 also agreed well with the experimental data, which validates the applicability of the adopted equivalent electrical circuits.

The fitting parameters for Fig. 9 are listed in Table 3. In this study, a total resistance (R_t) was used to characterize the anti-corrosion performance of copper, where R_t is defined as the sum of the corrosion products film resistance (R_f) and charge transfer resistance (R_{ct}). Obviously, the R_t values on both sides of the exposed samples were different. With the increase of exposure time, the R_t of the front side increased gradually, while the reverse trend was observed on the back side. Moreover, the R_t of the front side was significantly higher than that of the back side. These results demonstrate that the protection afforded by the corrosion product layer on the front side was improved gradually, while that on the back side was deteriorated. The EIS results were fairly consistent with the potentiodynamic polarization results in Fig. 8, proving the reliability of the electrochemical measurements.

4 Discussion

It is known that copper is an excellent corrosion resistant material; however, compared with other marine climate exposure fields, the average corrosion rate of copper T2 exposed in Nansha for one year was particularly high at 7.85 μm/a, indicating that Nansha has an extremely severe corrosive atmospheric environment. In addition, because of the different exposure orientations of the front and back sides of the samples, the atmospheric conditions endured by the two sides, such as the amount of sea salt deposition, rain erosion force and light irradiation intensity, were different. Therefore, corrosion mechanisms of the front and back sides of the exposed samples were also different.

When copper was exposed to the Nansha marine atmosphere, a thin electrolyte film could be formed on the sample due to sea salt deposition and dew-formation. The electrochemical dissolution of copper first occurred to form Cu^+ under the thin liquid layer:

$$4Cu+O_2+2H_2O\rightarrow 4Cu^++4OH^- \quad (2)$$

Subsequently, Cu^+ was transformed into the slightly soluble CuCl and soluble $CuCl_2^-$ in the presence of Cl^-, and most of the $CuCl_2^-$ was further converted to Cu_2O through precipitation as follows [31]:

$$2CuCl_2^-+2OH^-\rightleftharpoons Cu_2O+H_2O+4Cl^- \quad (3)$$

Table 3 Fitting results of EIS parameters for copper for different exposure time

Parameter	Front side				Back side			
	2 months	5 months	13 months	21 months	2 months	5 months	13 months	21 months
$R_s/(\Omega\cdot cm^2)$	6.83	10.00	5.68	8.80	13.78	8.28	15.63	6.20
$Q_f/(\Omega^{-1}\cdot s^n\cdot cm^{-2})$	3.04×10^{-6}	1.14×10^{-5}	4.99×10^{-7}	1.83×10^{-7}	2.55×10^{-5}	5.17×10^{-5}	1.29×10^{-4}	1.19×10^{-4}
n_f	0.6496	0.5395	0.6252	0.7869	0.5266	0.4545	0.4185	0.8791
$R_f/(\Omega\cdot cm^2)$	135.5	567.6	3914	592.2	81.64	287.3	171.7	229.7
$Q_{dl}/(\Omega^{-1}\cdot s^n\cdot cm^{-2})$	6.08×10^{-4}	1.26×10^{-4}	8.52×10^{-5}	3.48×10^{-5}	1.73×10^{-4}	1.07×10^{-4}	1.92×10^{-4}	2.42×10^{-4}
n_{dl}	0.5949	0.3865	0.5143	0.4021	0.6045	0.6667	0.4486	0.4249
$R_{ct}/(\Omega\cdot cm^2)$	2482	2626	3348	9014	1947	1363	1326	1095
$Z_w/(\Omega^{-1}\cdot s^{-0.5}\cdot cm^{-2})$	2.14×10^{-4}	7.53×10^{-4}	2.91×10^{-4}	4.19×10^{-4}	4.89×10^{-4}	6.68×10^{-4}	3.24×10^{-3}	1.09×10^{-2}
$R_t/(\Omega\cdot cm^2)$	2617.5	3193.6	7262.0	9606.2	2028.6	1650.3	1497.7	1324.7

The stability of Cu_2O is inversely dependent on the concentration of Cl^-. Due to the high salt environment in Nansha, the chloride ions would destroy the compact Cu_2O film on the copper surface to form soluble species, such as CuCl or $CuCl_2^-$. $CuCl_2^-$ produced was further oxygenated to $Cu_2Cl(OH)_3$ [14]:

$$3CuCl_2^- + 3/4O_2 + 3/2H_2O \rightarrow Cu_2Cl(OH)_3 + Cu^{2+} + 5Cl^- \quad (4)$$

Thus, the corrosion product layers with a double-layered structure were formed on the surface of copper: the inner layer was mainly composed of Cu_2O, in contact with the copper substrate; while the outer layer was mainly composed of $Cu_2Cl(OH)_3$, in contact with the environment. These processes resulted in a net release of OH^- on the copper surface. Considering the equilibrium between $Cu_2Cl(OH)_3$ and CuO, CuO was found to be stable at pH values above 8 [32,33]:

$$Cu_2Cl(OH)_3 + OH^- \rightleftharpoons 2CuO + 2H_2O + Cl^- \quad (5)$$

Because Nansha is in a rainy environment, it should be considered that the salt deposited on the front side of the exposed sample was diluted by rain, reducing the production of $Cu_2Cl(OH)_3$; further, the small amount of loose $Cu_2Cl(OH)_3$ that had formed on the front side was easily washed away, leading to an extremely thin outer layer and leaving a very compact and thick Cu_2O inner layer on the front side of copper. The compact products may act as a barrier to block the diffusion of the corrosive electrolyte and oxygen, resulting in a lower corrosion rate. Furthermore, this dense Cu_2O layer, which is a p-type semiconductor and thus has low electronic conductivity, was mainly responsible for the high resistance [34−36]. Therefore, a decreasing corrosion rate with exposure time was observed on the front side of copper due to the increased thickness of the Cu_2O layer.

However, the outer corrosion product layer on the back side gradually thickened. It has been generally accepted that the loose and very hygroscopic $Cu_2Cl(OH)_3$ layer can prolong the surface wetting time [13,37], thus accelerating the corrosion of copper. In addition, transverse cracks can be observed in the cross-sectional morphology on the back side (Fig. 6), indicating that the inner layer on the back side had poor adhesion with the matrix. The thick outer product layer and cracks can also trap water and provide a channel for the transport of the electrolyte film and oxygen to the surface of the substrate. These led to a decrease in the impedance of the corrosion product layer and severe corrosion on the back side.

In addition, with the continuous formation of corrosion products, the concentration of OH^- released on the copper surface also increased, resulting in a gradual increase in the pH. Therefore, black CuO compounds began to appear on the sample surface after 13 months of exposure. Since the back side was not susceptible to rain erosion, OH^- could be at a high concentration for a long time; consequently, the amount of CuO on the back side of copper was greater than that on the front side.

5 Conclusions

(1) Nansha has an extremely harsh marine atmospheric environment, classified as a corrosion category of CX. The thickness loss of copper obeyed a linear increase during the 21 months of exposure, and the average corrosion rate of copper exposed for one year was approximately 7.85 μm/a.

(2) The corrosion products formed on the copper surface mainly consisted of Cu_2O and $Cu_2Cl(OH)_3$. After 13 months of exposure, CuO was detected.

(3) The corrosion product layer formed on copper had a double-layered structure. The outer corrosion product layer on the front side was extremely thin because of rain erosion, while the outer product layer on the back side was thicker than the inner layer.

(4) The R_t values of the corrosion product layer on the front side increased as the exposure time increased, while the reverse trend was observed on the back side, indicating that the protection afforded by the corrosion product layer on the front side was improved gradually, while that on the back side was deteriorated.

Acknowledgments

The authors are grateful for the financial supports from National Natural Science Foundation of China (51671197) and Strategic Priority Research Program of Chinese Academy of Sciences (13040502).

References

[1] QI Dong-mei, CHENG Ruo-yi, DU Xiao-qing, CHEN Yu, ZHANG Zhao, ZHANG Jian-qing. Review on atmospheric corrosion of copper and copper alloys [J]. Journal of Chinese Society of Corrosion and Protection, 2014, 34(5): 389−398. (in Chinese)

[2] ARABAN V, KAHRAM M, REZAKHANI D. Evaluation of copper atmospheric corrosion in different environments of Iran [J]. Corrosion Engineering Science and Technology, 2016, 51(7): 498−506.

[3] SLAMOVA K, KOEHL M. Measurement and GIS-based spatial modelling of copper corrosion in different environments in Europe [J]. Materials and Corrosion−Werkstoffe Und Korrosion, 2017, 68(1): 20−29.

[4] KRATSCHMER A, WALLINDER I O, LEYGRAF C. The evolution of outdoor copper patina [J]. Corrosion Science, 2002, 44(3): 425−450.

[5] FONSECA I T E, PICCIOCHI R, MENDONCA M H, RAMOS A C. The atmospheric corrosion of copper at two sites in Portugal: A comparative study [J]. Corrosion Science, 2004, 46(3): 547−561.

[6] VERA R, ARAYA R, BAGNARA M, DIAZ-GOMEZ A, OSSANDON S. Atmospheric corrosion of copper exposed to different environments in the region of Valparaiso, Chile [J]. Materials and Corrosion, 2017, 68(3): 316−328.

[7] WAN Y, ZHANG H X, LI Y B, WANG X M, FAN Z R, ZHU X. Corrosion behaviors of copper exposed to an urban atmosphere [J]. International Journal of Electrochemical Science, 2018, 13(7): 6779−6790.

[8] LEYGRAF C, CHANG T, HERTING G, WALLINDER I O. The origin and evolution of copper patina colour [J]. Corrosion Science, 2019, 157: 337−346.

[9] ODNEVALL I, LEYGRAF C. Atmospheric corrosion of copper in a rural atmosphere [J]. Journal of the Electrochemical Society, 1995, 142(11): 3682−3689.

[10] SU W, LV W Y, LIU Z C, ZHANG Z G. Corrosion of copper exposed to Zhanjiang and Zhuhai atmospheric environments [J]. Anti-Corrosion Methods and Materials, 2017, 64(3): 286−292.

[11] ZHU Z P, ZUO X D, YING Z H. Corrosion analysis of copper T2 exposed to polluted atmospheres and study on prediction model [J]. Corrosion Reviews, 2017, 35(1): 35−46.

[12] WATANABE M, TOMITA M, ICHINO T. Characterization of corrosion products formed on copper in urban, rural/coastal, and hot spring areas [J]. Journal of the Electrochemical Society, 2001, 148(12): B522−B528.

[13] MENDOZA A R, CORVO F, GOMEZ A, GOMEZ J. Influence of the corrosion products of copper on its atmospheric corrosion kinetics in tropical climate [J]. Corrosion Science, 2004, 46(5): 1189−1200.

[14] CUI Zhong-yu, XIAO Kui, DONG Chao-fang, DING Yuan, WANG Tao, LI Xiao-gang. Corrosion behavior of copper and brass in serious Xisha marine atmosphere [J]. The Chinese Journal of Nonferrous Metals, 2013, 23(3): 742−749. (in Chinese)

[15] ZHANG X, WALLINDER I O, LEYGRAF C. Mechanistic studies of corrosion product flaking on copper and copper-based alloys in marine environments [J]. Corrosion Science, 2014, 85: 15−25.

[16] KONG D C, DONG C F, FANG Y H, XIAO K, GUO C Y, HE G, LI X G. Long-term corrosion of copper in hot and dry atmosphere in Turpan, China [J]. Journal of Materials Engineering and Performance, 2016, 25(7): 2977−2984.

[17] KONG D C, DONG C F, FANG Y H, XIAO K, GUO C Y, HE G, LI X G. Copper corrosion in hot and dry atmosphere environment in Turpan, China [J]. Transactions of Nonferrous Metals Society of China, 2016, 26(6): 1721−1728.

[18] AN Bai-gang, ZHANG Xue-yuan, HAN En-hou. Corrosion behavior of pure copper during initial exposure stage in atmosphere of Shenyang city [J]. Acta Metallurgica Sinica, 2007, 43(1): 77−81. (in Chinese)

[19] CAO Chu-nan. Material natural environmental corrosion of China [M]. Beijing: Chemical Industry Press, 2005. (in Chinese)

[20] WAN S, MA X Z, MIAO C H, ZHANG X X, DONG Z H. Inhibition of 2-phenyl imidazoline on chloride-induced initial atmospheric corrosion of copper by quartz crystal microbalance and electrochemical impedance [J]. Corrosion Science, 2020, 170: 108692.

[21] YUAN S J, PEHKONEN S O. Surface characterization and corrosion behavior of 70/30 Cu−Ni alloy in pristine and sulfide-containing simulated seawater [J]. Corrosion Science, 2007, 49(3): 1276−1304.

[22] CHENG Y L, ZHANG Z, CAO F H, LI J F, ZHANG J Q, WANG J M, CAO C N. A study of the corrosion of aluminum alloy 2024-T3 under thin electrolyte layers [J]. Corrosion Science, 2004, 46(7): 1649−1667.

[23] KING F, QUINN M J, LITKE C D. Oxygen reduction on copper in neutral NaCl solution [J]. Journal of Electroanalytical Chemistry, 1995, 385(1): 45−55.

[24] LIAO X N, CAO F H, ZHENG L Y, LIU W J, CHEN A N, ZHANG J Q, CAO C N. Corrosion behaviour of copper under chloride-containing thin electrolyte layer [J]. Corrosion Science, 2011, 53(10): 3289−3298.

[25] VERA R, DELGADO D, ROSALES B M. Effect of atmospheric pollutants on the corrosion of high power electrical conductors−Part 2. Pure copper [J]. Corrosion Science, 2007, 49(5): 2329−2350.

[26] TOUZ E, COUGNON C. Study of the air-formed oxide layer at the copper surface and its impact on the copper corrosion in an aggressive chloride medium [J]. Electrochimica Acta, 2018, 262: 206−213.

[27] LI H T, CHEN Z Y, LIU X C, HOU J, SUN M X, ZENG R C. Study on the mechanism of the photoelectrochemical effect on the initial NaCl-induced atmospheric corrosion process of pure copper exposed in humidified pure air [J]. Journal of the Electrochemical Society, 2018, 165(10): C608−C617.

[28] WAN S, MIAO C H, WANG R M, ZHANG Z F, DONG Z H. Enhanced corrosion resistance of copper by synergetic effects of silica and BTA codoped in polypyrrole film [J]. Progress in Organic Coatings, 2019, 129: 187−198.

[29] ZERJAV G, MILOSEV I. Protection of copper against corrosion in simulated urban rain by the combined action of

benzotriazole, 2-mercaptobenzimidazole and stearic acid [J]. Corrosion Science, 2015, 98: 180−191.

[30] PAN C, GUO M X, WANG Z Y. Effect of $MgCl_2$ on the corrosion behavior of copper under periodic wet/dry cycle condition [J]. Journal of Materials Engineering and Performance, 2019, 28(5): 2562−2572.

[31] KEAR G, BARKER B D, WALSH F C. Electrochemical corrosion of unalloyed copper in chloride media—A critical review [J]. Corrosion Science, 2004, 46(1): 109−135.

[32] STRANDBERG H, JOHANSSON L G. Some aspects of the atmospheric corrosion of copper in the presence of sodium chloride [J]. Journal of the Electrochemical Society, 1998, 145(4): 1093−1100.

[33] LIN H, FRANKEL G S. Atmospheric corrosion of Cu during constant deposition of NaCl [J]. Journal of the Electrochemical Society, 2013, 160(8): C336−C344.

[34] RICE D W, PETERSON P, RIGBY E B, PHIPPS P B P, CAPPELL R J, TREMOUREUX R. Atmospheric corrosion of copper and silver [J]. Journal of the Electrochemical Society, 1981, 128(2): 275−284.

[35] DRUSKA P, STREHBLOW H H, GOLLEDGE S. A surface analytical examination of passive layers on CuNi alloys. Part I: Alkaline solution [J]. Corrosion Science, 1996, 38(6): 835−851.

[36] WATANABE M, HIGASHI Y, TANAKA T. Differences between corrosion products formed on copper exposed in Tokyo in summer and winter [J]. Corrosion Science, 2003, 45(7): 1439−1453.

[37] MANSFELD F, LIU G, XIAO H, TSAI C H, LITTLE B J. The corrosion behavior of copper-alloys, stainless-steels and titanium in seawater [J]. Corrosion Science, 1994, 36(12): 2063−2095.

铜在中国南沙群岛极端恶劣海洋大气中的腐蚀行为

路 肖[1,2]，刘雨薇[1,2]，赵洪涛[2]，潘 晨[2]，王振尧[2]

1. 中国科学技术大学 材料科学与工程学院，沈阳 110016；
2. 中国科学院 金属研究所，沈阳 110016

摘 要：通过质量损失法、成分分析、形貌观察和电化学测试等手段，研究纯铜在南沙大气中暴露 21 个月后的腐蚀行为。结果表明，铜暴露一年的平均腐蚀速率约为 7.85 μm/a，这意味着南沙群岛属于 CX 腐蚀等级。在暴露样品的正反两面形成的腐蚀产物层的结构和性能差异很大。正面的腐蚀产物层内层(Cu_2O)较厚且致密，外腐蚀产物层($Cu_2Cl(OH)_3$)极薄；而样品反面的外产物层却比内层厚。电化学测试结果表明，正面腐蚀产物层提供的防护作用逐渐增强，而反面腐蚀产物层的防护作用逐渐减弱。

关键词：铜；现场暴露；质量损失；大气腐蚀；南沙群岛

(Edited by Bing YANG)